Observation of vortex dynamics in arrays of nanomagnets

W. Yu[1], P.S. Keatley[1], P. Gangmei[1], M. K. Marcham[1], T. H. J. Loughran[1], R. J. Hicken[1], S.A. Cavill[2,3], G. van der Laan[2], J.R. Childress[4], and J.A. Katine[4]

[1] *School of Physics and Astronomy, University of Exeter, Stocker Road, Exeter EX4 4QL, United Kingdom*

[2] *Diamond Light Source, Harwell Science and Innovation Campus, Didcot, Oxfordshire OX11 0DE, United Kingdom*

[3] *Department of Physics, University of York, York, YO10 5DD, United Kingdom*

[4] *HGST, San Jose Research Center, 3403 Yerba Buena Road, San Jose, California 95135, USA*

Abstract

Vortex dynamics within arrays of square ferromagnetic nano-elements have been studied by time-resolved scanning Kerr microscopy (TRSKM), while x-ray photoemission electron microscopy has been used to investigate their equilibrium state. An alternating field demagnetization process was found to initialize a distribution of equilibrium states within the individual elements of the array, including quasi-uniform states and vortex states of different chirality and core polarization. Repeated initialization revealed some evidence of stochastic behaviour during the formation of the equilibrium state. TRSKM with a spatial resolution of ~300 nm was used to detect vortex gyration within arrays of square nano-elements of 250 nm lateral size. Two arrays were studied consisting of a 9×9 and 5×5 arrangement of nano-elements with 50 nm and 500 nm element edge-to-edge separation to encourage strong and negligible dipolar interactions respectively. In the 5×5 element array, TRSKM images, acquired at a fixed phase of the driving microwave magnetic field, revealed differences in the gyrotropic phase within individual elements. While some phase variation is attributed to the dispersion in the size and shape of elements, the vortex chirality and core polarization are also shown to influence the phase. In the 9×9 array, strong magneto-optical response due to vortex gyration was observed across regions with length equal to either one or two elements. Micromagnetic simulations performed for 2×2 arrays of elements suggest that particular combinations of vortex chirality and polarization in neighbouring elements are required to generate the observed magneto-optical contrast.

I. INTRODUCTION

The gyrotropic mode[1,2,3,4,5] of a magnetic vortex[6] is currently the subject of intense research because microwave emission from a spin torque vortex oscillator (STVO) has a tuneable frequency[7,8,9] and narrow linewidth[10] that is attractive for microwave signal processing applications. While the emitted power from a single STVO is too small to be of widespread technological use, it may be enhanced by careful consideration of the device materials,[11] or by mutual synchronization of multiple STVOs so that the power level can be increased.[12,13,14] Phase locking has only been demonstrated for a small number of STVOs that share a common magnetic layer[12,14] or that are injection locked to the same microwave current source.[13] For multiple isolated STVOs the dynamic dipolar interaction between the gyrotropic modes of the individual devices[15] also has the potential to phase lock and synchronise their dynamic response without the need for common layers or additional interconnects. However to understand the formation of collective gyrotropic modes within large arrays, it is first necessary to image the dynamics of individual elements, pairs, and smaller arrays so that the character of the collective modes may be determined.

Recently, investigations of dynamically coupled magnetic vortices have been reported in pairs,[16,17,18,19,20,21,22] trios,[23] chains,[22,24] and arrays[25,26,27,22,28] of microscale ferromagnetic disks and squares. In large arrays of ~300 microscale discs, ferromagnetic resonance experiments revealed broadening of the vortex gyrotropic mode as the separation between the elements was decreased,[25] suggesting increased splitting of a large number (~300) of unresolved collective modes. At the same time, time-resolved magneto-optical Kerr effect measurements were used to detect the splitting of collective gyrotropic modes within arrays of 250 microscale discs, which was shown, with the aid of micromagnetic simulation, to be due to inter-element magnetostatic coupling mediated by uncompensated magnetic charge near to the edges of the elements.[26] Most of these studies investigate coupled vortex dynamics in microscale magnetic elements, while in STVOs nanoscale magnetic elements are necessary in order to achieve suitable current density to excite the gyrotropic mode using spin transfer torque. To that end it is a necessary prerequisite to investigate the dynamic response of magnetic vortices in arrays of nanoscale elements.

In this work we used time-resolved scanning Kerr microscopy (TRSKM) to detect the vortex gyrotropic mode of individual nanomagnets within arrays, and x-ray photoemission electron microscopy (XPEEM) to determine their equilibrium state. The arrays were initialized by applying a slowly alternating in-plane magnetic field of decreasing amplitude. By imaging the polar Kerr signal at a fixed point in the microwave cycle, the phase of vortex gyration within the elements of the array can be detected. Two arrays consisting of 250 nm square elements in a 5×5 and 9×9 configuration with respective edge-to-edge separations of 500 nm and 50 nm were considered. Time-resolved (TR) Kerr images acquired from the 9×9 array show that the magneto-optical contrast can extend across small regions of the array corresponding to a pair of elements. Micromagnetic simulations of 2×2 arrays reveal that the observed magneto-optical contrast can be described by a specific equilibrium configuration of the vortex chirality and core polarization, which have previously been shown to lead to different eigenmodes of interacting microscale discs.[23]

II. EXPERIMENT AND SAMPLE DETAILS

A multilayer stack of composition Ta(5)/Cu(25)/[Ta(3)/Cu(25)]$_3$/Ta(10)/Ru(5)/ $Ni_{81}Fe_{19}$(40)/Al(1.5) (thicknesses in nm), was sputtered onto an insulating sapphire wafer of 500 μm thickness. The NiFe layer was protected from oxidation by a self-passivating Al capping layer that was allowed to oxidise naturally in air. Four repeats of Cu laminated with Ta provided a thick (~100 nm) metallic underlayer that was used to fabricate an integrated coplanar waveguide. At the same time the lamination helps to maintain a flat surface for the deposition of NiFe that can be difficult to achieve with Cu alone. Arrays of permalloy squares were formed on the Cu underlayer by a combination of electron beam lithography and ion beam milling. The remaining Cu/Ta underlayers were patterned by photolithography and ion beam milling to form a coplanar waveguide (CPW) such that the arrays of nano-elements were located on top of a narrow section of the central conductor with length 2.29 mm and width 6 μm. The width of the central conductor and its separation from the surrounding ground planes were designed to achieve a characteristic impedance of 50 Ω on the sapphire substrate. A schematic of the coplanar waveguide structure is shown in Figure 1(a). Magnetization dynamics were excited using the in-plane magnetic field associated with pulsed or microwave (RF) current waveforms passing through the narrow section of the CPW. A NiCr thin film resistor with DC resistance of ~ 50 Ω was deposited at one end of the CPW to attenuate the time-varying current and prevent multiple reflections.

TRSKM was used to study the coupled vortex dynamics of square 250×250 nm^2 nanomagnets within two arrays with edge-to-edge separations of 500 nm and 50 nm. The vortex equilibrium state was generated in the nano-elements by applying a slowly (<1 Hz) alternating in-plane magnetic field with continuously decreasing amplitude. A Ti:sapphire oscillator was used to generate optical pulses of ~100 fs duration, 800 nm wavelength and 80 MHz repetition rate. Second harmonic generation was then used to generate a 400 nm (blue) optical probe that was expanded (×5) to reduce beam divergence, before being linearly polarized, and then focused to a diffraction limited spot diameter of ~ 300 nm using a high numerical aperture (0.85, ×60) microscope objective lens.[29] TR measurements were made by using a 4 ns optical delay line to change the relative phase of the optical pulses and the pulsed or RF field excitation generated by the CPW at the sample position. The amplitude of the excitation was modulated at a frequency of ~3 kHz. The Kerr rotation was measured using a balanced photodiode polarizing bridge detector, with a lock-in amplifier to recover the modulated signal component. TR Kerr images were acquired at a fixed phase of RF field excitation by scanning the sample beneath the focussed spot using a piezoelectric scanning stage. The microscope had sufficient spatial resolution and long term mechanical stability to detect magnetization dynamics within the individual nanomagnets of the arrays.

TRSKM is a stroboscopic technique that reveals only changes in the magnetic state. Therefore additional information about the equilibrium magnetic state is required to correctly interpret the TRSKM data. XPEEM was used to image the equilibrium vortex states in nominally identical arrays to those used in the TRSKM measurements. The XPEEM images were acquired at the I06 Nanoscience beamline at the Diamond Light Source, UK. X-rays with an energy corresponding to the L_3 absorption edge of Fe were used to acquire images of the in-plane magnetization, using x-ray magnetic circular dichroism (XMCD) as the contrast mechanism.[30] The spatial resolution of the XPEEM used for this study was ~50 nm, in a geometry that allowed the projection of the in-plane component of the magnetization onto the x-ray wavevector to be imaged.

III. RESULTS AND DISCUSSION

A. Static and dynamic measurements of single microscale elements

Since the elements within the arrays have a length that is smaller than the focused spot size in the TRSKM, it is necessary to first confirm that the magnetic field initialization generates a vortex equilibrium state within square elements. In Figure 1(b) an XPEEM image of a 10 μm square demonstrates sensitivity to the Landau flux closure domains that are associated with a vortex core at the centre of the element. The formation of the vortex in larger elements with very small aspect ratio (thickness/lateral size) d/L of ~0.004 suggests that the field initialization is suitable for vortex nucleation in the smaller elements, with larger d/L of ~0.16, within the arrays.[31] The black and white contrast in the XPEEM image corresponds to the in-plane component of the equilibrium magnetization that lies parallel or anti-parallel to the x-ray wavevector respectively. In Figure 1(b) the grey regions have magnetizations that lie perpendicular to the x-ray wavevector, so that the magnetization rotates in the plane of the square forming a vortex core at the center. In elements with length greater than the focused spot size, TRSKM can be used to observe the vortex state by detecting higher frequency magnetization precession within the surrounding flux closure domains. In Figure 1(c) a TR Kerr image of the vortex state in a 1 μm square is shown. The white and black contrast respectively to the left and to the right of the center of the square results from the out-of-plane torque of opposite sign acting on the two closure domains with magnetization perpendicular to the pulsed magnetic field **h**(t). In Figure 1(d) TR signals acquired from these two domains are almost identical, but for their opposite sign. Therefore, in smaller squares, for which the optical spot size is similar to, or larger than the structure, the net polar Kerr signal due to precession within the domains may be negligible. In fact, in an ideal symmetric element the polar Kerr signal due to vortex gyration is also expected to be negligible since there is no net change in the out-of-plane component of the dynamic magnetization that can be detected by TRSKM as the vortex gyrates within the region of the optical probe.

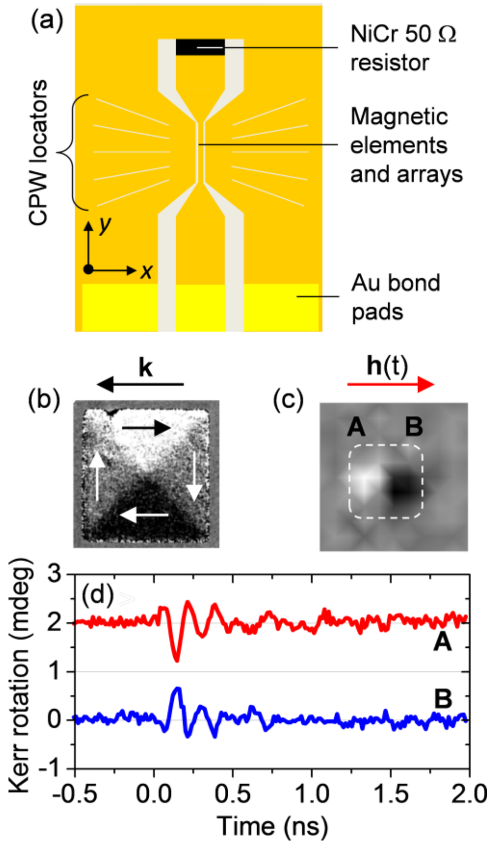

Figure 1. (color online) (a) Schematic of the CPW structure with the location of the magnetic elements and arrays indicated in the narrow section. (b) An XPEEM image of a Landau flux closure state in a 10 μm square. Arrows within the figure denote the in-plane magnetization direction. (c) TR Kerr image of a 1 μm square. (d) TR Kerr signals acquired at positions A and B in (c). The TR image in (c) was acquired at the first antinode of precession.

However, detection of the vortex gyration using TR polar Kerr microscopy is possible, and has previously been reported in sub-micron sized disks probed by a 500 nm diameter spot.[2,3,5] In the following we review how the vortex gyration is observed using this technique.

In Figure 2(a) the measured (black trace) and simulated[32] (blue trace) out-of-plane component of the dynamic magnetization of a 500 nm square is shown in response to an in-plane pulsed field. The experimental TR Kerr signal shows the low frequency vortex gyration superimposed upon the higher frequency precessional modes of the closure domains.[2,3] The experimental data was acquired with a 300 nm diameter focused spot that yields the average out-of-plane component of the dynamic magnetization within the probed area. In micromagnetic simulations, when the components of the dynamic magnetization are averaged across the entire area of the square, only higher frequency modes that possess a spatially symmetric component are observed in the out-of-plane magnetization, while the low frequency gyration of the vortex core is only observed in the in-plane magnetization components. However, if the dynamic magnetization is averaged over a $250\times250\ \mathrm{nm}^2$ region, of roughly similar area to that of the optical probe in the experiment, that is slightly displaced from the center of the square (inset graphic Figure 2(a)), the vortex gyration can be observed in the out-of-plane component as in the experiment. This result implies that detection of vortex gyration using the polar Kerr effect in a TRSKM measurement requires a small displacement of the optical probe with respect to the centre of the square. Since the beam intensity has a Gaussian profile, a net polar Kerr signal due to the vortex gyration is observed even when the element is smaller than the spot size, as long as the center of the beam is displaced relative the center of the element.

In Figure 2(a) the higher frequency oscillations of the simulated TR trace have smaller amplitude relative to the smoothed (red) trace than observed in the experiment. The relative amplitude is likely to be affected by the position, area, shape, and profile of the region of interest in the simulation, in addition to the pulsed field amplitude. Fast Fourier transform (FFT) spectra in Figure 2(b) show that the overall dynamic response is well reproduced by the simulation. Spatial maps of the FFT power spectra calculated from the micromagnetic simulation[33] confirm that the lowest frequency mode (~500 MHz) is the vortex gyrotropic mode (V), while the higher frequency modes (1 to 4) are found to be associated with oscillations of the domain walls separating the Landau closure domains (5 GHz),[2] and higher frequency azimuthal modes with at least one nodal plane in each closure domain (6.7 GHz, 8.2 GHz, and 10 GHz).

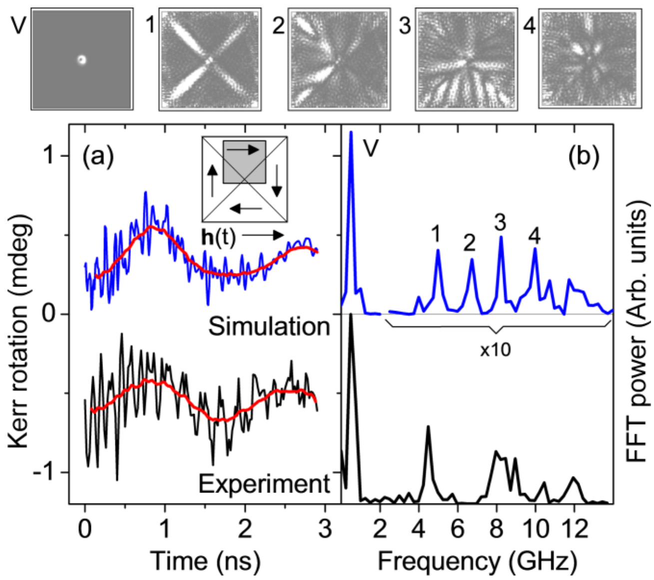

Figure 2. (Color online) (a) Measured and simulated TR traces of the out-of-plane component of the dynamic magnetization acquired from a single 500 nm square in the vortex state in response to a pulsed magnetic field. The simulated trace is extracted from the 250 nm square region shown in the inset. (b) FFT power spectra corresponding to the TR traces in (a). The inset images (V, 1 to 4) show the spatial distribution of the FFT power spectra calculated from the simulations.

B. Dynamic measurements of arrays

To study the dynamic interaction of vortices within the arrays, TRSKM with sub-GHz RF field excitation was used to excite only the gyrotropic mode. The higher frequency spin waves of the confined in-plane magnetization, as observed in Figure 2 in response to a broadband pulsed field excitation, are not excited by the sub-GHz RF field excitation. The array with largest edge-to-edge separation (500 nm) was studied first so that the response of individual isolated 250×250 nm^2 nanomagnets could be detected. The output power of the RF synthesiser was maintained at 25 dBm for all measurements. In Figure 3(a) typical TR polar Kerr signals acquired from a single square within the array, highlighted by the black circle in the scanning electron microscope (SEM) image inset in Figure 3(b), are shown

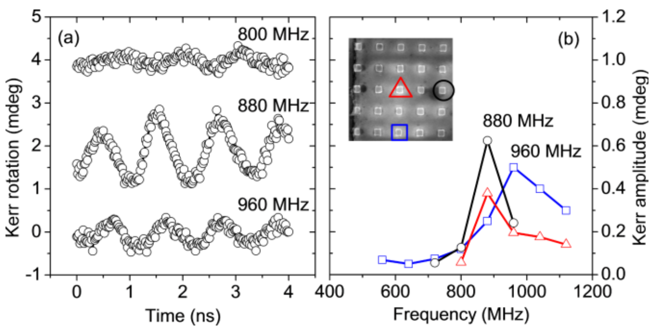

Figure 3. (Color online) (a) The measured TR Kerr signals are shown with different RF frequency for the square element indicated by the black circle within the SEM image in panel (b). The line and symbol curves in panel (b) show the frequency dependence of the Kerr amplitude for the elements highlighted by the same symbol within the SEM image.

for three different values of the RF frequency. The largest amplitude response, corresponding to the resonance frequency of the vortex gyrotropic mode, was found to be at 880 MHz. The aspect ratio d/L of the square nano-elements studied in this work was ~0.16. The corresponding resonance frequency of the vortex gyrotropic mode expected from the empirical formula given in Reference 34 is 867 MHz. In

Figure 3(b) the Kerr amplitude for three different elements within the array is shown as a function of the RF frequency and found to vary from element-to-element. A resonance frequency of ~880 MHz was observed in two (black circle and red triangle) of the three elements shown, with the linewidth and amplitude somewhat different in all three elements. While these differences might result from the weak interactions of an element with its nearest neighbours, the gyration frequency also depends strongly on the aspect ratio of the element. As such these differences are more likely due to variations in the size and shape of individual elements. For example, the element (blue square) with a resonance frequency of 960 MHz in Figure 3(b) corresponds to an element size of 276 nm according to Reference 34. Note that the observed frequencies in Figure 3(b) are slightly larger than those predicted by Reference 34 suggesting that the elements are slightly larger than the nominal size of 250 nm. The linewidth of the vortex gyrotropic mode is expected to be smaller than the frequency resolution of the TRSKM, which is limited by the 80 MHz laser repetition rate. Therefore, the variation in resonance frequency between 880 MHz and 960 MHz, the linewidth, and lineshape, is consistent with a small variation of the lateral size of the magnetic element between 250 nm and 276 nm.

In Figure 4(a) two TR Kerr images of the array containing 250 nm squares with 500 nm edge-to-edge separation are shown for two points in the RF cycle separated by π radians (labelled + and –). The frequency of the RF excitation was 960 MHz. It is clear that some elements are missing from the TR images, but where elements are visible, variations in the amplitude and orientation of the black and white contrast of the Kerr signal can be seen. The black and white contrast results from the amplitude modulation of the excitation, as illustrated in Figure 4(e). At a particular point in the cycle of the RF excitation, the vortex core will be at a corresponding point on its trajectory away from the center of the element. The effect of amplitude modulation is then detected in TRSKM measurements as a change of the out-of-plane component of the magnetization (ΔM_z) as the vortex core ‘jumps’

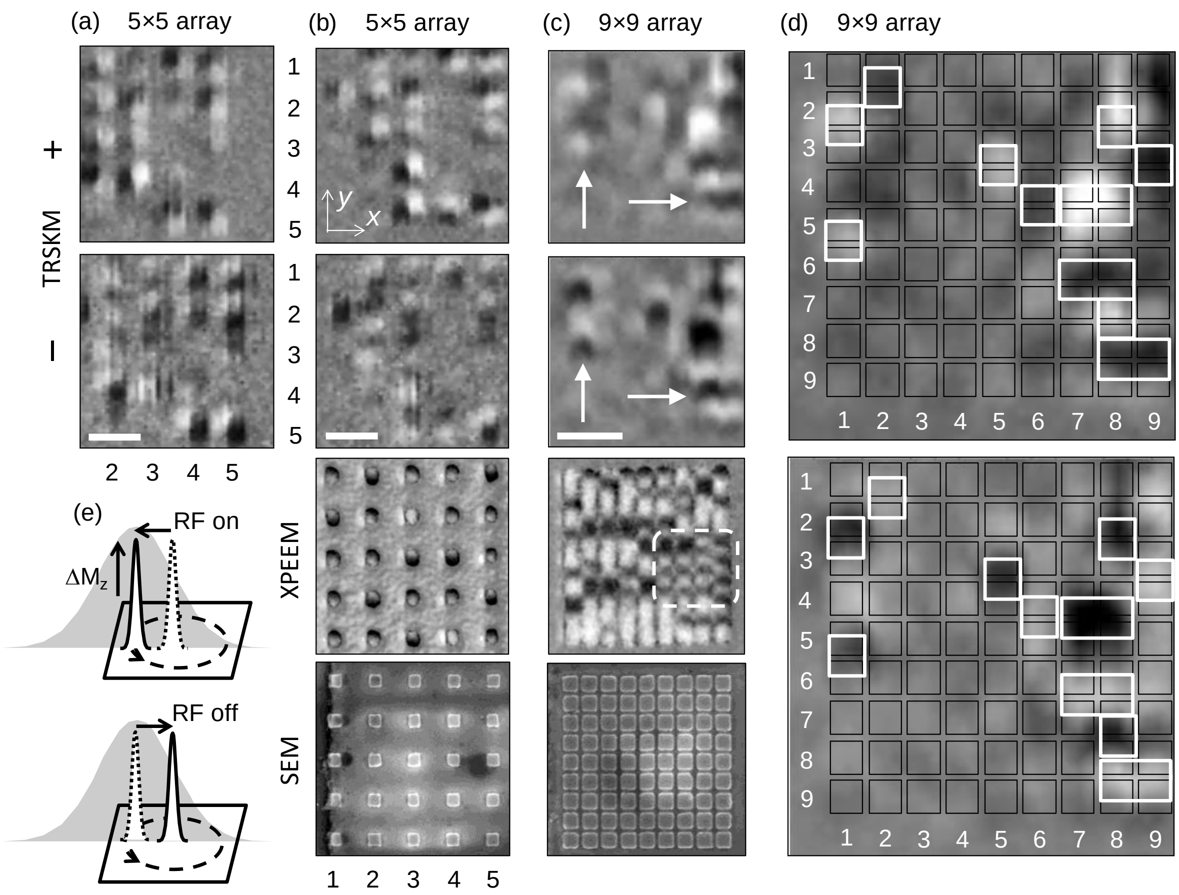

Figure 4. TRSKM images, XPEEM images and SEM images of arrays of 250 nm squares with separation of 500 nm in (a) and (b), and 50 nm in (c). After acquisition of the TRSKM images in (a), the equilibrium state was re-initialized before acquiring the TRSKM images in (b). In all TRSKM images the horizontal white bar has length of 1 µm. In (c) the white arrows in the TRSKM images denote regions of contrast with size comparable to, or larger than that of a single element, while the dashed white rectangle in the XPEEM image highlights a cluster of elements with vortex equilibrium states. (d) enlarged view of (c), in which the black grid position is a guide to the eye to show where the individual elements lie, and the white boxes highlight regions of contrast that are either 1×1 or 2×1 elements in size. In (a), (b) and (d) the rows and columns of numbers form a coordinate system by which the squares are referred to in the main text. All TRSKM images are shown at antinodes of opposite polarity (labelled + and –) in the TR signal acquired from the square in the top-right corner of each array. (e) Schematic illustration of how the magneto-optical contrast arises. The solid curves represent the polar magnetization component of the vortex core, while the grey shading represents the Gaussian intensity profile of the focused optical probe.

from the center of the element (equilibrium state, RF excitation off) to the particular point on the trajectory (gyrotropic state, RF excitation on). When the core jumps from the center to the edge of the element in this way, a corresponding decrease (increase) of the polar Kerr signal can be observed when the optical probe is near to the center (edge) of the element. As the phase of the excitation changes, the regions of black and white contrast rotate about the centre of the element, as confirmed by TR images acquired at antinodes of opposite polarity. In that way the orientation of the observed polar Kerr contrast for each element is related to the gyrotropic phase of the vortex core.

In the following discussion, different squares within the array will be referred to by their (column, row) coordinates. In Figure 4(a) column 1 lay outside the scanning range. The TR images were acquired at time delays corresponding to antinodes of opposite polarity in the polar Kerr signal acquired from square (5, 1). It is clear that the black and white contrast corresponding to vortex gyration is not observed in all elements within the array. For example squares (2, 5), (3, 5), (4, 3), and (5, 4) appear to be missing. These 'missing' squares have a quasi-uniform single domain ground state that supports confined spin wave modes with frequency typically greater than 2 GHz at remanence[33,35] and so no response is observed at 960 MHz. Comparison of Figure 4(a) and Figure 4(b) reveal that the formation of the vortex state was not reproducible in all squares. When the ground state of the array was reset, the majority of squares remained in the vortex state, but square (3, 5) adopted the vortex state generating a detectable signal, while squares (4, 2), (4, 4), and (2, 4) adopted the single domain state yielding no signal at 960 MHz. Element (3, 4) in Figure 4(a) and elements (3, 4) and (3, 5) in Figure 4(b) also appear with stronger contrast than other elements. This suggests slight differences in the radius of the vortex core gyration due the variation of resonance frequencies in accordance with element size (aspect ratio).

In the lower panel of Figure 4(b) a normalized XMCD image of a nominally identical 5×5 array is shown. The dark and light contrast in the XMCD image corresponds to the in-plane equilibrium magnetization that lies parallel and anti-parallel to the x-ray wavevector in the –*x* direction. The XMCD image reveals that element (3, 2) and (4, 5) have a single domain state, which supports the interpretation of the missing elements in Figure 4(a) and Figure 4(b). In the remaining elements, approximately one half of each element is dark, while the other half is light, which reveals that the majority of elements adopt the vortex state.

After the initialization process used to prepare the equilibrium state of the array shown in Figure 4(a) was repeated, many of the elements that retained the vortex state appeared to have similar contrast and therefore phase of gyration, Figure 4(b). For a small number of elements, differences in the contrast were observed following re-initialization. In Figure 4(a), elements (4, 5) and (5, 5) have similar phase of gyration, while element (3, 5) is missing. In Figure 4(b) element (3, 5) now occupies a vortex state while the orientation of the contrast of (4, 5) has changed by π radians. The vortex state has four different configurations corresponding to the possible permutations of the chirality[36] of the in-plane magnetization and the vortex core polarization. For the same excitation conditions, the sense of gyration, i.e. clockwise or counter-clockwise, is determined by the core polarization only.[37] Alternatively vortex states with the same core polarization, but opposite chirality exhibit a constant gyrotropic phase difference of π radians during the cycle. Therefore, the phase difference in the orientation of the polar Kerr contrast of a pair of elements can vary between 0 and π radians when the elements have the same chirality, but opposite core polarization (sense of gyration), and a constant phase difference of π radians when the core polarization of each element is the same, but their chirality is opposite. Initialization of the equilibrium state by sweeping an in-plane magnetic field with decreasing amplitude does not allow the chirality or core polarization of the vortex state to be selected. However the π phase shift in (4, 5) suggests that the core polarization, the chirality, or both characteristics switched during the re-initialization of the equilibrium state, in agreement with micromagnetic simulations. To determine which characteristics of the vortex state switched during re-initialization, TR Kerr images with phase resolution better than $\pi/2$-radians would be required. In Figure 4(b) the XPEEM image of the 5×5 array reveals that the vortex chirality is not strongly correlated from element-to-element. While it is not possible to extract the core polarization from the XPEEM images, the image clearly shows that nearest neighbours may adopt vortex states with the same or opposite chirality. This supports the interpretation that the different orientation of the contrast observed from element-to-element in the TR Kerr images of Figure 4(a) and 4(b) are associated with the presence of vortices of different chirality and polarization.

In elements (3, 4) and (4, 5) the orientation of the contrast is different by about $\pi/2$ radians for both field histories and may alternatively be the result of a difference in size or shape between these two elements since the resonance frequency depends upon the aspect ratio.[34] In a real array, the aspect ratio is expected to vary from element-to-element. Micromagnetic simulations of a 250×250 nm^2, 40 nm thick, square element show that resonant excitation of the gyrotropic mode, by an in-plane RF field of frequency 990 MHz, can yield an off-resonance response in a second element with a size that differs from that of the first element by as little as 10 nm.

The off-resonance response is known to have a different trajectory and exhibit a phase difference of up to $\pi/2$ radians with respect to the on-resonance response[38] leading to the smaller phase differences in the contrast of individual elements in Figure 4(a) and Figure 4(b).

In the 5×5 array, the dipolar interaction is not expected to have a significant influence on the vortex state configuration due to the with large edge-to-edge separation (twice the element length). The change in the equilibrium states of a small number of elements for a repeated field history (described earlier) does not appear to be controlled by the initialization process, or correlated with nearest neighbour elements. This suggests that thermal effects, edge defects, and surface roughness may influence the nucleation process in the 5×5 array, or perhaps a recently reported asymmetry in the formation process that may arise from an intrinsic Dzyaloshinskii–Moriya interaction.[39]

In Figure 4(c), similar TR Kerr images were acquired from a 9×9 array of 250 nm squares with 50 nm edge-to-edge separation for which the static and dynamic dipolar interactions between elements are expected to be enhanced. While the spatial resolution of the TRSKM is insufficient to observe the individual elements within the array, remarkably, regions of alternating TR Kerr signal (indicated by the white arrows) are observed that appear to extend over length scales that are equal to or larger than the individual element size. Figure 4(d) shows an enlarged view of Figure 4(c) in which black grids have been positioned to guide the eye to the physical boundaries of the elements, while the white boxes highlight regions of contrast that are either 1×1 or 2×1 elements in size. For example, a region of contrast extending over 2×1 elements overlaps elements (7, 4), (7, 5), (8, 4) and

(8, 5), while a 1×1 region of contrast is observed between elements (9, 3) and (9, 4). As observed for the 5×5 array with larger separation, the 9×9 array exhibits regions with no obvious Kerr signal at a RF frequency of 960 MHz, for example in the lower-left quadrant of the array. This is consistent with the XPEEM image in the bottom panel of Figure 4(c) of a nominally identical 9×9 array, which shows that many of the elements occupy a quasi-uniform single domain state. In measurements of the vortex nucleation and annihilation magnetic fields in chains of closely spaced sub-micron square elements, the vortex state was found to be destabilized as the inter-element separation was reduced.[40] This is reflected in the comparison of the XPEEM images of the 5×5 and 9×9 arrays for which the proportion of vortex states is reduced in the latter array with smaller separation. While the 50 nm spacing between individual elements was not fully resolved, the vortex states of individual elements are still clearly seen within the XPEEM image. Elements with uniform contrast over a length scale of a single element in the *y*-direction occupy single domain states, while elements with contrast variation (dark and light) over the same length scale in the *y*-direction occupy a vortex state. The XPEEM image in Figure 4(c) shows a large cluster of vortex states located at the middle of the right-hand edge of the array (indicated by the dashed white rectangle). The two right-most columns of elements within the dashed white rectangle reveal vortex states of opposite circulation, which is seen as a half-element-length spatial shift in the *y*-direction of the dark and light contrast in the two coliumns. While an exact correspondence with the equilibrium states observed by TRSKM is not expected, the appearance of clusters of elements in the vortex state is qualitatively similar.

C. Micromagnetic simulations

Micromagnetic simulations[32] were performed to interpret the TR Kerr images by considering five different combinations of vortex equilibrium configurations within a 2×2 array of square elements. The nominal dimensions for the film thickness (40 nm), element size (250 nm), and edge-to-edge separation (50 and 500 nm) were used. A cell size of 5×5×40 nm^3 and an exchange parameter of 13×10^{-7} erg/cm were used. The saturation magnetization and g-factor were assumed to have values of 800 emu/cm^3 and 2.1 respectively. While a Gilbert damping parameter α of about 0.01 is typically observed for permalloy, a value of 0.001 was assumed so as to yield smaller linewidths allowing mode splitting to be more easily identified. The vortex state of each element was prepared by defining four closure domains with uniform in-plane magnetization and a circular core with uniform out-of-plane magnetization. The five regions were exchange coupled and allowed to relax in zero external magnetic field. Initially the value of α was set to 0.5 to allow the magnetization to relax more efficiently. Pulsed magnetic field simulations were then performed with a pulse defined as the product of the functions $f(t) = 1 - \exp(-\frac{t}{\tau_1})$ and $g(t) = -\exp(-\frac{t-t_0}{\tau_2})$, where t_0 = 70 ps, τ_1 = 50 ps, and τ_2 = 40 ps, so as to yield a full width half maximum (FWHM) pulse width of 70 ps and a full rise time (0-100%) of 30 ps. The pulse shape is shown in the inset of Figure 5(b) and is similar to that used to excite the vortex gyrotropic mode in the experiment presented in Figure 2(a). Vector maps of the magnetization were recorded over a period of 100 ns at 0.05 ns intervals. The out-of-plane component of the magnetization for each element was averaged over its lower half only, so as to yield a non-vanishing time-dependent signal from the gyrotropic mode.

Figure 5(a) shows simulated TR signals corresponding to the out-of-plane component of the dynamic magnetization M_z for each element of a simulated 2×2 array of 250 nm squares with 50 nm spacing. Each column represents a different equilibrium configuration of the vortex states within the array, as shown in the schematics at the top of each column that are labelled 1 to 5. In each column, four TR signals are shown corresponding to the average response of M_z in the lower half of the highlighted squares (white) in the schematic of the 2×2 array to the right of the TR signals.

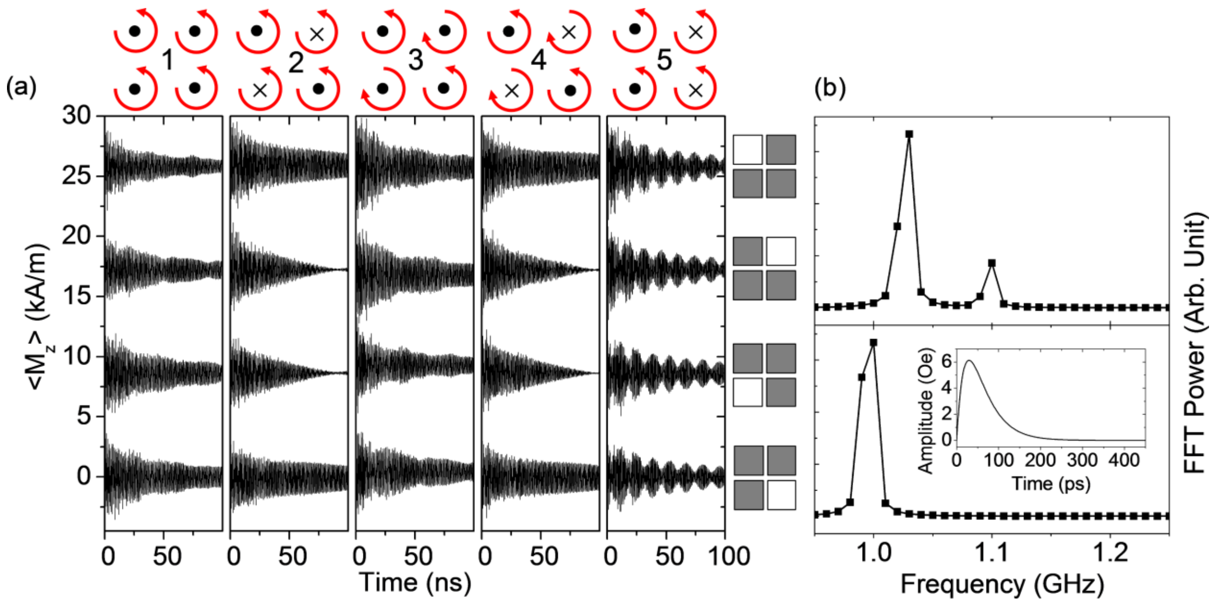

Figure 5 (colour online) (a) out-of-plane magnetization (M_z) sampled from the bottom half of each element within a 2×2 array of 250 nm squares with 50 nm spacing. White squares on the right side of the plot denote the element positions within the array. The red arcs denote the chirality of the vortex state, while the black dots and crosses denote the vortex polarization. (b) Normalized FFT power spectra for the upper left element in configuration 5, with the upper and lower panel showing the FFT power spectra from the arrays with 50 and 500 nm separation respectively. The inset figure in the lower panel denotes the pulse shape used in the simulation.

The evolution of the TR signals is markedly different for the five equilibrium configurations. TR signals from all four elements in configuration 5 exhibit beating

(Figure 5(a), column 5) with frequency of ~ 70 MHz. Since TRSKM with RF excitation has a frequency resolution of 80 MHz, it is not expected that the modes giving rise to the beating can be resolved experimentally. In configurations 2 and 4, the amplitude of the TR signals from the upper-right and lower-left elements of the arrays decays much faster than those from the upper-left and lower-right elements. While the chirality of the in-plane magnetization in these two elements is of opposite sign, the sign of vortex core polarization is the same. Since the sense of the gyrotropic motion is governed by the polarization only, we look in more detail at equilibrium configuration 4 only, since that of configuration 2 is found to yield a very similar dynamic response, as shown by the TR signals in Figure 5(a).

In configurations 1 and 3, the TR signals from all elements exhibit a qualitatively similar non-exponential relaxation, but without any clear beating. In fact closer inspection reveals that there are similarities in the TR traces, albeit with minor differences in their amplitude. In the two configurations (1) and (3) the response of the upper(1) and lower(3) left elements are similar with opposite chirality; the response of the upper(1) and lower(3) right elements are similar with the same chirality; the response of the lower(1) and upper(3) left elements are similar with the same chirality; and finally the response of the lower(1) and upper(3) right elements are similar with opposite chirality. While the chirality does not change the sense of gyration, it does lead to a π radian phase difference in the core position on the trajectory and may therefore lead to the formation of collective modes of the 2×2 array due to the magnetostatic dipolar coupling described previously. However, the coupling is weaker than for equilibrium configurations 2 and 4, and significantly weaker than configuration 5. Therefore, splitting of the gyrotropic mode in configurations 1 to 4 was not observed in the fast Fourier transform spectra of the

TR traces presented in Figure 5(a). Indeed the splitting in configuration 5 was shown to be as little as 70 MHz, Figure 5(b).

These features all point to the influence of magnetostatic dipolar interactions between the elements. Interestingly, the largest effects, beating in configuration 5 and variations in relaxation in configurations 2 and 4, occur when the array contains elements with different core polarization, suggesting that the core polarization drives the inter-element interactions. Therefore, we concentrate on the more interesting configurations 4 and 5. These observations are in agreement with theoretical studies[20,22,28] that point out that the vortex eigen-frequencies of interacting disks do not depend on the direction of the in-plane chirality of the vortex magnetization, but strongly depend on the out-of-plane vortex core polarizations. Since the core polarization governs the sense of gyration, a corresponding change in the inter-element magnetostatic coupling mediated by uncompensated magnetic charge takes place.[26]

In Figure 5(b), FFT spectra are shown for the top-left element in configuration 5 for edge-to-edge separations of 50 nm (upper panel) and 500 nm (lower panel), as used in the experiment. For a separation of 500 nm the spectrum shows a single peak with frequency of 0.99 GHz, at which the elements within the two columns gyrate with opposite sense. For the smaller separation of 50 nm two modes with frequencies of 1.03 GHz and 1.10 GHz are observed, for which the 70 MHz splitting corresponds to the beat frequency observed in the time domain. Further simulations of arrays with element separations of 100 and 200 nm showed that the splitting of these modes decreased until they could not be resolved for a separation of 500 nm. For the dominant lower frequency mode, elements within the two columns again gyrate with opposite sense. The character of the other possible collective modes will not be considered any further here, since the aim of the present study is only to explain the results of the TRSKM study.

In the experiments, amplitude modulation was applied to the RF waveform used to excite the sample. Therefore TRSKM was used to probe the change in the out-of-plane component of the dynamic magnetization with respect to the equilibrium state, as shown schematically in Figure 4(e). To understand how the equilibrium state configuration of the densely packed arrays can lead to the magneto-optical contrast observed experimentally in Figure 4(c), images of the difference between the dynamic and equilibrium magnetization maps were calculated.

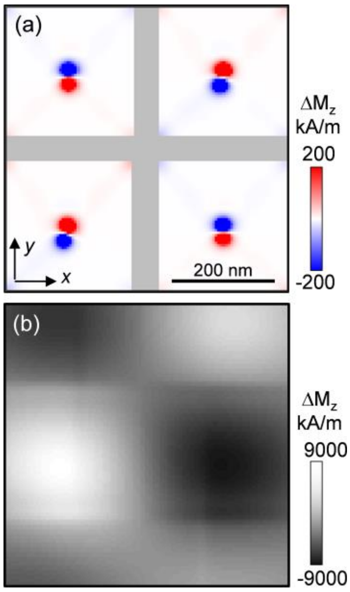

Figure 6 (colour online) (a) Spatial variation of the change of the out-of-plane magnetization (ΔM_z) induced by the RF excitation, for an array with 50 nm separation in configuration 4 of Figure 5. (b) Convolution of the ΔM_z image with a two dimensional Gaussian function with FWHM of 300 nm.

Figure 6(a) shows a magnetization difference image for the vortex gyrotropic mode for an array with 50 nm edge-to-edge separation with equilibrium configuration 4 as shown in Figure 5(a). The in-plane RF driving field had frequency of 960 MHz and amplitude of 5 Oe, while the value of the Gilbert damping parameter α was set to be 0.01. The pair of elements in the column on the left-hand side of the array shows red contrast towards the center of the pair, while the pair in the right-hand column shows blue contrast towards their center. The red and blue contrast corresponds to a positive and negative change in the out-of-plane component of the dynamic magnetization respectively. To understand the signal obtained by scanning a 300 nm diameter laser spot across the centre of the array, and to afford direct comparison with the experimental results, the calculated ΔM_z image was convolved with a 2-D Gaussian function with FWHM of 300 nm. In the convolved image of Figure 6(b), regions of black and white contrast with similar size to that of an individual element are observed at the centre of the array. Therefore in Figure 4(c), the origin of regions of contrast that extend over the area of about one element size can be understood from changes in M_z of the same sign that occur towards the near-side edges of adjacent elements. However, the TRSKM images in Figure 4(c) reveal that in at least one region, black, or alternatively white, contrast can extend over a length equivalent to 2×1 elements. Figure 7 again shows difference images for a 2×2 element array with 50 nm edge-to-edge separation, but now for equilibrium configuration 5 (Figure 5(a)) subject to an in-plane RF-field excitation at 1.03 GHz with amplitude of 5 Oe. Images are shown for four different points in the RF cycle, with the sense of gyration in each element being indicated by the arrows. At a time delay of 1.6 ns (2.1 ns) all four of the blue (red) regions lie closer to the vertical centreline of the array. Repeating the convolution procedure used in Figure 6(b), it is seen that black, or alternatively white, contrast now extends across a length of two elements in the vertical direction and one element in the horizontal direction at certain points in the RF cycle (1.6 and 2.1 ns). This explains the appearance of regions of similar contrast of 2×1 size in Figure 4(c) and (d).

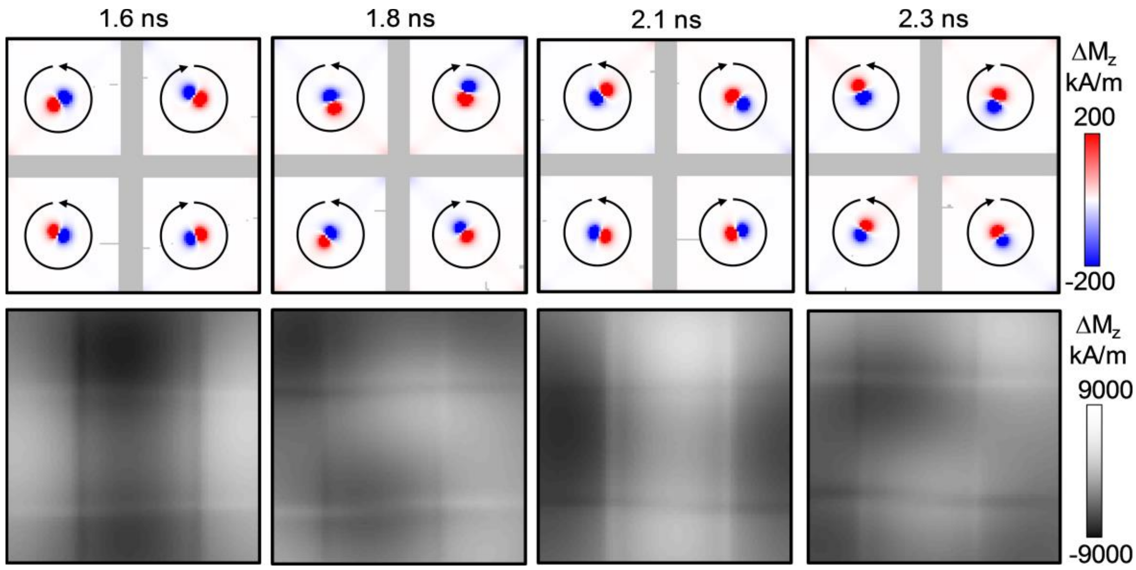

Figure 7 (colour online) Upper panels show the spatial distribution of the change of the out-of-plane magnetization ΔM_z induced by RF excitation at a frequency of 1.03 GHz . The elements in the 2×2 array have 50 nm separation and equilibrium state corresponding to configuration 5 in Figure 5. Black arcs denote the sense of gyration of the vortex. The lower panels show the expected form of the magneto-optical signal calculated in a similar manner as in Figure 6 as described within the main text.

In Figure 4(d), three regions of contrast with size equal to 2×1 elements may be seen, of which one is somewhat stronger than the others. The observed beating in the TR traces of configuration 5 corresponds to a 70 MHz variation in the radius of the core trajectory. For the particular region that exhibits the strongest contrast the elements are likely to be precisely on resonance and exhibit the largest displacement of the vortex core as the amplitude of the RF field is modulated. Consequently, it should be expected that small variations in the element shape, size, or magnetic parameters will lead to variations of the collective resonances throughout the array. This will be of significant importance for magnonic devices, that may well rely upon a more uniform dynamic response.

IV. SUMMARY

TRSKM has been used to detect vortex gyration in individual square nanomagnets with lateral size smaller than the focused spot diameter. TR Kerr images revealed differences in the phase of vortex gyration within individual elements of a 5×5 array with 500 nm edge-to-edge separation for which inter-element dipolar interactions are expected to be weak. The observed orientation of the polar Kerr contrast in neighbouring elements can differ by up to π radians as a result of opposite vortex chirality and/or core polarizations. At the same time smaller variations of up to $\pi/2$ radians are also present that suggest small variations of element aspect ratio, which has a strong influence on the gyrotropic eigen-frequency. The distribution of equilibrium states within the elements may be influenced by nanoscale structural imperfections, but thermal effects were also shown to play a role since different equilibrium states were obtained when the same field initialization process was repeated. Control of the equilibrium states requires a more elaborate initialization process, preferably at the level of an individual element, in which an out-of-plane field is used to control the core polarization[41] and a spatially inhomogeneous in-plane field, perhaps due to exchange bias, controls the chirality. TR Kerr images of a 9×9 array with 50 nm edge-to-edge separation revealed regions of uniform contrast extending over lengths comparable to that of either one or two by one elements. Simulations of 2×2 arrays showed that the spatial extent of regions of uniform contrast depends strongly on the equilibrium configuration of vortex chirality and core polarization within individual elements. For certain equilibrium configurations, the simulations also revealed noticeable frequency splitting of the gyrotropic mode. The present work therefore demonstrates the rich magnetization dynamics that may be achieved by controlling the chirality and polarization of vortices within an array of nanomagnets. More extensive micromagnetic simulations, that explore the large number of possible equilibrium states, are now required both to understand the character of the collective gyrotropic modes that may occur, and to fully reproduce the character of TR images observed experimentally.

Acknowledgements

The authors thank G. Hrkac for stimulating discussion on the origin of the contrast observed in TR Kerr images, and gratefully acknowledge financial support from the EU Grant MASTER No. NMP-FP7-212257, and the UK Engineering and Physical Sciences Research Council (EPSRC) Grant Reference EP/I038470/1.

References

[1] K.Y. Guslienko, B.A. Ivanov, V. Novosad, Y. Otani, H. Shima, and K. Fukamichi, Journal of Applied Physics **91**, 8037 (2002).

[2] J. Park, P. Eames, D. Engebretson, J. Berezovsky, and P. Crowell, Physical Review B **67**, 020403 (2003).

[3] J. Park and P. Crowell, Physical Review Letters **95**, 167201 (2005).

[4] S.-B. Choe, Y. Acremann, A. Scholl, A. Bauer, A. Doran, J. Stöhr, and H.A. Padmore, Science **304**, 420 (2004).

[5] X. Zhu, Z. Liu, V. Metlushko, P. Grütter, and M.R. Freeman, Physical Review B **71**, 180408 (2005).

[6] T. Shinjo, T. Okuno, R. Hassdorf, K. Shigeto, and T. Ono, Science **289**, 930 (2000).

[7] M.R. Pufall, W.H. Rippard, M.L. Schneider, and S.E. Russek, Physical Review B **75**, 140404 (2007).

[8] Q. Mistral, M. van Kampen, G. Hrkac, J.-V. Kim, T. Devolder, P. Crozat, C. Chappert, L. Lagae, and T. Schrefl, Physical Review Letters **100**, 257201 (2008).

[9] T. Devolder, J.-V. Kim, P. Crozat, C. Chappert, M. Manfrini, M. van Kampen, W. Van Roy, L. Lagae, G. Hrkac, and T. Schrefl, Applied Physics Letters **95**, 012507 (2009).

[10] V.S. Pribiag, I.N. Krivorotov, G.D. Fuchs, P.M. Braganca, O. Ozatay, J.C. Sankey, D.C. Ralph, and R.A. Buhrman, Nat Phys **3**, 498 (2007).

[11] A. Dussaux, B. Georges, J. Grollier, V. Cros, A.V. Khvalkovskiy, A. Fukushima, M. Konoto, H. Kubota, K. Yakushiji, S. Yuasa, K.A. Zvezdin, K. Ando, and A. Fert, Nat Commun **1**, 8 (2010).

[12] A. Ruotolo, V. Cros, B. Georges, A. Dussaux, J. Grollier, C. Deranlot, R. Guillemet, K. Bouzehouane, S. Fusil, and A. Fert, Nature Nanotechnology **4**, 528 (2009).

[13] A. Dussaux, A.V. Khvalkovskiy, J. Grollier, V. Cros, A. Fukushima, M. Konoto, H. Kubota, K. Yakushiji, S. Yuasa, K. Ando, and A. Fert, Applied Physics Letters **98**, 132506 (2011).

[14] S. Sani, J. Persson, S.M. Mohseni, Y. Pogoryelov, P.K. Muduli, A. Eklund, G. Malm, M. Käll, A. Dmitriev, and J. Åkerman, Nature Communications **4**, 2731 (2013).

[15] A. Belanovsky, N. Locatelli, P. Skirdkov, F. Abreu Araujo, J. Grollier, K. Zvezdin, V. Cros, and A. Zvezdin, Physical Review B **85**, 100409 (2012).

[16] S. Sugimoto, Y. Fukuma, S. Kasai, T. Kimura, A. Barman, and Y. Otani, Physical Review Letters **106**, 197203 (2011).

[17] S. Jain, H. Schultheiss, O. Heinonen, F.Y. Fradin, J.E. Pearson, S.D. Bader, and V. Novosad, Physical Review B **86**, 214418 (2012).

[18] A. Vogel, T. Kamionka, M. Martens, A. Drews, K.W. Chou, T. Tyliszczak, H. Stoll, B. Van Waeyenberge, and G. Meier, Physical Review Letters **106**, 137201 (2011).

[19] H. Jung, K.-S. Lee, D.-E. Jeong, Y.-S. Choi, Y.-S. Yu, D.-S. Han, A. Vogel, L. Bocklage, G. Meier, M.-Y. Im, P. Fischer, and S.-K. Kim, Sci. Rep. **1** (2011).

[20] J. Shibata, K. Shigeto, and Y. Otani, Physical Review B **67**, 224404 (2003).

[21] O.V. Sukhostavets, J.M. Gonzalez, and K.Y. Guslienko, Applied Physics Express **4**, 065003 (2011).

[22] O. Sukhostavets, J. González, and K.Y. Guslienko, Physical Review B **87**, 094402 (2013).

[23] X. Wang, D.J. Keavney, M. Asmat-Uceda, K.S. Buchanan, A. Melikyan, and X.M. Cheng, Applied Physics Letters **105**, 102408 (2014).

[24] D.-S. Han, A. Vogel, H. Jung, K.-S. Lee, M. Weigand, H. Stoll, G. Schutz, P. Fischer, G. Meier, and S.-K. Kim, Sci. Rep. **3** (2013).

[25] A. Vogel, A. Drews, T. Kamionka, M. Bolte, and G. Meier, Physical Review Letters **105**, 037201 (2010).

[26] A. Barman, S. Barman, T. Kimura, Y. Fukuma, and Y. Otani, Journal of Physics D: Applied Physics **43**, 422001 (2010).

[27] M. Hänze, C.F. Adolff, M. Weigand, and G. Meier, Applied Physics Letters **104** (2014).

[28] J. Shibata and Y. Otani, Physical Review B **70**, 012404 (2004).

[29] P.S. Keatley, P. Gangmei, M. Dvornik, R.J. Hicken, J. Grollier, C. Ulysse, J.R. Childress, and J.A. Katine, Topics in Applied Physics **125**, 17 (2013).

[30] D.E. Parkes, R. Beardsley, S. Bowe, I. Isakov, P.A. Warburton, K.W. Edmonds, R.P. Campion, B.L. Gallagher, A.W. Rushforth, and S.A. Cavill, Applied Physics Letters **105** (2014).

[31] M. Schneider, H. Hoffmann, S. Otto, T. Haug, and J. Zweck, Journal of Applied Physics **92**, 1466 (2002).

[32] M. Donahue and D.G. Porter, OOMMF User's Guide, Version 1.0, NISTIR 6376 (National Institute of Standards and Technology, Gaithersburg, MD, 1999): see http://math.nist.gov/oommf.

[33] P.S. Keatley, V.V. Kruglyak, A. Neudert, E.A. Galaktionov, R.J. Hicken, J.R. Childress, and J.A. Katine, Physical Review B **78**, 214412 (2008).

[34] A. Vansteenkiste, J. De Baerdemaeker, K.W. Chou, H. Stoll, M. Curcic, T. Tyliszczak, G. Woltersdorf, C.H. Back, G. Schütz, and B. Van Waeyenberge, Physical Review B **77**, 144420 (2008).

[35] G. Gubbiotti, M. Madami, S. Tacchi, G. Carlotti, A.O. Adeyeye, S. Goolaup, N. Singh, and A.N. Slavin, Journal of Magnetism and Magnetic Materials **316**, 338 (2007).

[36] We use the term chirality to refer to the in-plane circulation of the magnetization since the upper and lower surfaces are inequivalent and so define a handedness. This is not to be confused with the definition of the chirality as the product of the circulation and the core polarization.

[37] M. Curcic, B. Van Waeyenberge, A. Vansteenkiste, M. Weigand, V. Sackmann, H. Stoll, M. Fähnle, T. Tyliszczak, G. Woltersdorf, C.H. Back, and G. Schütz, Physical Review Letters **101**, 197204 (2008).

[38] K.-S. Lee and S.-K. Kim, Physical Review B **78**, 014405 (2008).

[39] M.-Y. Im, P. Fischer, K. Yamada, T. Sato, S. Kasai, Y. Nakatani, and T. Ono, Nat Commun **3**, 983 (2012).

[40] V. Novosad, M. Grimsditch, J. Darrouzet, J. Pearson, S.D. Bader, V. Metlushko, K. Guslienko, Y. Otani, H. Shima, and K. Fukamichi, Applied Physics Letters **82**, 3716 (2003).

[41] S. Jain, V. Novosad, F.Y. Fradin, J.E. Pearson, V. Tiberkevich, A.N. Slavin, and S.D. Bader, Nat Commun **3**, 1330 (2012).